Available online at www.sciencedirect.com

ScienceDirect

Applied Energy

A Generalized Quasi-Dynamic Model for Electric-Heat Coupling Integrated Energy System with Distributed Energy Resources

Xin Qin[a], Hongbin Sun[a,b] , Xinwei Shen[a,*], Ye Guo[a], Qinglai Guo[a,b], Tian Xia[b]

[a]*Tsinghua-Berkeley Shenzhen Institute, Tsinghua University, 1001 Xueuan Blvd., Shenzhen 518055, China*
[b]*Department of Electrical Engineering, Tsinghua University, Rm. 3-120 West Main Building, Beijing 100084, China*

Abstract

The deployment of the electric-heat coupling Integrated Energy System (IES) with distributed energy resources (DERs) integrated has benefited the environment for improving energy efficiency and reducing carbon emission. The accurate calculation of IES power flow helps to meet the demand of users better and quantify the flexibility of IES for accommodating more renewables. However, modeling and calculating the power flow of IES become challenging because of the DERs and the different characteristics of electricity and heat such as system dynamic process, network topology and control mechanism. To overcome the challenges in existing IES model, this paper proposes a generalized quasi-dynamic model and a decomposition-iteration solving method for the electric-heat coupling IES, which considers the heat dynamic process, meshed network topology, multiple DERs and variable mass flow simultaneously. From the results of case studies, the proposed IES model has the average error of 0.09% compared with real measured data and surpasses commercial software in terms of pipe temperature dynamics, which demonstrates the accuracy and generality of the proposed model. Moreover, with several numerical tests, convergence analysis for the proposed model is also provided.

Highlights:
1. The power flow of electric-heat coupling Integrated Energy System is analyzed.
2. Model is divided into several parts and solved sequentially and iteratively.
3. Convergence analysis shows outstanding computational stability of proposed model.
4. Average error of proposed model is only 0.09% compared with real measurements.
Keywords: combined heat and power; district heat network; power flow; convergence analysis; heat dynamic process; distributed energy resource

1. Introduction

With environmental benefits such as high efficiency and low emission, the electric-heat coupling Integrated Energy System (IES) [1], also known as combined electricity and heat system and Multi-Energy System [2], has been deployed all over the world. It has been reported that IES can improve about 50% of fuel efficiency and reduce 13%~18% of carbon emission by recycling heat [3][4]. Meanwhile, by equipping distributed energy resources (DERs) such as renewable and biomass [5], the environmental friendliness of the IES can be further improved. Besides, the IES has various and large-scale application scenarios in the real world. For example, the combined heat and power (CHP) units in the northern Europe and northern China have already contributed 30~50% of regional electric power production [6][7], while the U.K. has an ambitious plan on deploying distributed CHP units to meet local electric and heat demand in the plan of "Thousands of Flowers" [8][9]. To ensure the energy supply quality of users and exploit the flexibility of IES for accommodating more renewables, it is essential to calculate the IES power flow accurately so that the IES operation state can be better estimated.

However, since the IES couples two different energy systems i.e. electric power system (EPS) and district heating system (DHS), which have diverse characteristics, modeling the IES and calculating IES power flow become very complicated especially when multiple DERs are integrated into IES. Firstly, as shown in Fig. 1, because electricity and heat have different dynamic processes, i.e. time scales, when

* Corresponding author. Xinwei Shen, Tel.: +86-13554871126.
E-mail address: sxw.tbsi@sz.tsinghua.edu.cn
The short version of the paper was presented at ICAE2018, Aug 22-25, Hong Kong. This paper is a substantial extension of the short version of the conference paper.

the EPS has already reached steady state in milliseconds, the thermal process of DHS is still in dynamic process [10][11]. It is challengeable to solve a set of complicated equations where variables of nonlinear electric and hydraulic equations are coupled with variables of partial differential thermal equations. Secondly, EPS and DHS have different network topologies including the meshed network and multiple DERs [12], which cause nonlinearity. Thirdly, considering EPS and DHS have different control mechanisms for reliability and efficiency, variables of EPS and DHS are time-varying e.g. operators adjust mass flow in DHS to improve efficiency [13][14], but this leads to nonlinearity in model formulation and challenges existing solving methods.

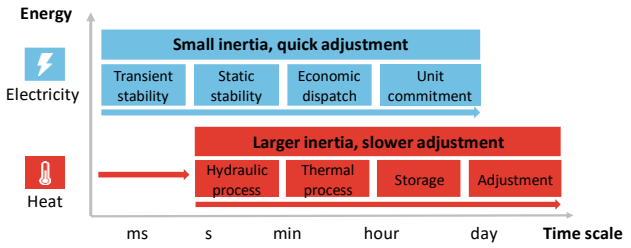

Fig. 1. The time scales of different energy systems.

To overcome these challenges, researchers have made unremitting efforts. Here, based on whether the DHS dynamic process in IES is considered, the models of IES are divided into two types: the steady-state model [9,14-18] and the dynamic model [13,19-25]. If not specified, the "model" may include IES model and corresponding solving method.

The steady-state model assumes that both EPS and DHS in IES have no dynamic process. Based on this assumption, [15] and [16] optimized the IES using the simplified steady-state model which ignores electric and heat network. [17] proposed the Energy Hub model to describe energy conversion between different energies, and this method can be applied in arbitrary topology for modeling and optimization [18]. [19] considered simple network constraints in design-operation optimization. However, both electric and heat networks are ignored or simplified as fixed transmission coefficients in [15-19], neglecting the consideration of IES power flow. The simplification leads to the fact that the results of above models are relatively rough and may break the network limits such as the transmission capacity, the voltage limit and the supply temperature limit. Thus, energy supply may have poor quality and fail to meet the demand of users. To take network into account, [20] proposed a steady-state model for electric-heat coupling IES considering meshed network, multiple DERs and variable mass flow, and [21] extended this model to combined electricity, heat and gas system. [10] analyzed the interaction of EPS and DHS in an electric-heat coupling IES with variable mass flow, meshed heat network and multiple DERs based on the model in [20], while [22] took the detailed EPS and DHS network into consideration during IES planning. However, the model in [10,20-22] does not consider the heat dynamic process in DHS. As a result, the results are inaccurate in terms of time and spaces, and the flexibility of IES cannot be fully exploited, which contraries to the motivation of deploying IES.

The dynamic model aims to address the heat dynamic process analysis of DHS simplified by the steady-state model. Researchers have developed model-driven methods [14, 23-31] and data-driven methods [32][33]. In the first category, [23] validated the dynamic thermal model for a pipe in [24] based on a virtual heating system. Nevertheless, the model just analyzed one pipe in the DHS rather than the system, and the same is true of [25]. [26] proposed a DHS model in which thermal dynamic process and variable mass flow are considered, but it only considers the simple network with a single pipe connecting a single DER and a single user. Based on a real-world IES network with loops, [27] developed a quasi-dynamic DHS model, but how to deal with direction-varying mass flow and changing mixing node still needs to be further explored. Besides, [22-27] only analyzes the power flow of a single DHS without EPS in IES. To analyze the interaction of EPS and DHS in the dynamic process, [28] developed a quasi-dynamic system model, but the model does not consider multiple DERs and direction-varying mass flow, which has the similar problems as [14]. [29], [30] and [31] expanded the quasi-dynamic IES model to the meshed DHS network with multiple DERs, however, the pipe mass flow is fixed at the constant rate. Meanwhile, to overcome the complexity of modeling IES with the dynamic process, some researchers developed the second category models i.e. data-driven models. [32] proposed a black-box compact physical model to calculate IES power flow which overcomes the nonlinearity caused by the meshed DHS network. [33] built an individual-based model to reflect the dynamic heat process of IES and analyze power flow. However, these data-driven methods need massive and detailed data to train and cannot guarantee the accuracy and generality under different circumstances.

In summary, current models for the IES impose different assumptions on the IES. To make it clear, the remaining challenges are presented in Table. 1.

Table 1

Unsolved Problems in Existing Literature

Challenges	Assumptions
Electric-heat coupling	Separating EPS and DHS [23,25-27]
IES dynamic process	Assuming IES has no dynamic process [16,17-21]
Network topology	Assuming radial network or single DER in DHS [14,23,25,26]
Control mechanism	Fixing mass flow in DHS [29,30]

The aim of this paper is to propose a generalized IES model with the calculation method, in which heat dynamic process, meshed network topology, multiple DERs and direction-variable mass flow are considered simultaneously. An iterative solving method is developed to decompose complicated interrelated equations from different models into small parts and solve them iteratively. Convergence of the proposed model is analyzed mathematically and numerically. Based on the data from a real DHS, the literature and the commercial software, case studies demonstrate the effectiveness of the proposed model. The

conclusion of this work is summarized finally. The comparison of the proposed method in this paper and other typical research is presented in Table 2, and the contribution of this research is summarized as follows:

1) A generalized electric-heat coupling IES model is proposed considering the heat dynamic process, meshed network topologies, multiple DERs and direction-variable mass flow simultaneously.
2) The solving method decomposes the complicated IES model into small parts based on the physical nature of IES.
3) The convergence is analyzed mathematically and numerically to illustrate computational stability.
4) Data from different sources are applied to validate the proposed model and demonstrate the effectiveness.

2. Model Formulation

The IES consists of two diverse energy systems i.e. EPS and DHS, which are mainly coupled at sources. In this session, the quasi-dynamic models of the EPS and the DHS in IES are formulated based on mature research, where the DHS has the hydraulic process and the thermal process. In minutes, the EPS and the hydraulic process in DHS have already reached the steady state while the thermal process in DHS is still in dynamic process [10], therefore, the IES model is established according to this physical nature, which is called the quasi-dynamic model.

2.1 Model of Electric Power System

The EPS model aims to describe the relationship between electric variables. Based on the well-known alternating current (AC) power flow equations, the EPS model can be applied in the arbitrary electric network with multiple DERs, including CHP unit, thermal unit, photovoltaic, wind power and biomass [34]. The variables of EPS are bus voltage, phase angle, active power and reactive power.

The voltage of the bus *i* is denoted by

$$V_{i,t} = |V_{i,t}|(\cos\theta_{i,t} + j\sin\theta_{i,t}) \tag{1}$$

where $|V_{i,t}|$ and $\theta_{i,t}$ are the voltage magnitude and phase angle of bus *i* at time *t*. And the *i* is for $\forall i \in E$, in which the *E* is the set of buses in EPS.

The injecting complex power, active power and reactive power of bus *i* are calculated by

$$S_{i,t} = P_{i,t} + jQ_{i,t} = V_{i,t}\sum_{j=1}^{N_e}(Y_{ij}V_{j,t})^* \tag{2}$$

where $S_{i,t}$, $P_{i,t}$ and $Q_{i,t}$ are the complex power, the active power and the reactive power of bus *i* at time *t* respectively. The Y_{ij} indicates the admittance from node *i* to *j*, and the N_e is the bus number in EPS.

2.2 Model of CHP units and other DERs

This section aims to illustrate the coupling of electricity and heat. As shown in (3), the CHP units and other DERs such as thermal generator can be modeled as the model of CHP units [14][20], whose feasible region are described using the polyhedrons reflecting the relation between electric power and heat power

$$P_{i,t} = \sum_{k=1}^{NK_i}\alpha_{i,t}^k P_i^k,\ \ \Phi_{i,t} = \sum_{k=1}^{NK_i}\alpha_{i,t}^k \Phi_i^k \tag{3}$$

where P_i^k and Φ_i^k are *k*th extreme points in the feasible operating region of the electric and heat power output for CHP unit *i*, respectively. $\Phi_{i,t}$ is the heat power output of CHP unit *i* at time *t*. The $\alpha_{i,t}^k$ should satisfy

$$\sum_{k=1}^{NK_i}\alpha_{i,t}^k = 1,\quad 0 \le \alpha_{i,t}^k \le 1$$

where NK_i is the number of extreme points in the feasible operating region of CHP unit *i*. Eq. (3) indicates that the electric power output and heat output are interrelated at sources.

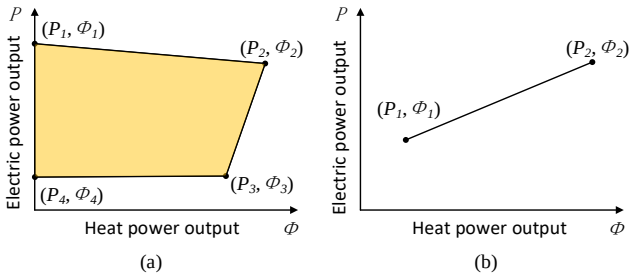

Fig. 2. The feasible region of (a) extraction condensing CHP unit and (b) back pressure CHP unit.

For example, Fig. 2 (a) and Fig. 2 (b) present the models of an extraction condensing CHP unit and a back-pressure CHP unit respectively [38]. It is also noteworthy that a thermal unit can be modeled as a CHP unit with zero heat output, and a heat pump can be modeled as a CHP unit with the negative electric output.

Table 2

Comparison of the proposed model and current typical models

	Electric-heat coupling	Heat dynamic process	Multi-DERs	Arbitrary topology	Variable mass flow
X Liu-J Wu'16-APEN [20]	√	×	√	√	√
Z Li-M Shahidehpour' 15-TSE [14]	√	√	×	×	√ (only >0)
W Gu-J Wang'17-APEN [30]	√	√	√	√	×
I B Hassine'13-APTE [27]	×	√	×	√	√ (only >0)
The proposed model	√	√	√	√	√

2.3 Model of District Heating System

This section aims to formulate the quasi-dynamic DHS model, which includes the steady-state hydraulic model and the dynamic thermal model. The DHS consists of heat source, heat load, supply pipe and return pipe, and the variables in DHS are mass flow, node pressure and pipe pressure drop in the hydraulic model and node supply temperature, node return temperature, pipe initial temperature and pipe terminal temperature in the thermal model.

2.3.1 Steady-state Hydraulic Network Model

The aim of the hydraulic model is to get mass flow and pressure distribution of the DHS network. The hydraulic model is based on Kirchhoff's law [37], which is similar to that in EPS and is compared in Table 3.

Table 3

The comparison of Kirchhoff's law in hydraulic model and EPS model

Kirchhoff's law in	Calculating node	Calculating loop	Calculating single branch
EPS model	Kirchhoff's current law	Kirchhoff's voltage law	Ohm's law
Hydraulic model	Continuity of flow equation	Pressure drop equation	Head loss equation

Firstly, the continuity of flow equation is expressed as: the mass flow consumed at a node equals to the minus of the mass flow injecting into the node and the mass flow leaving from the node

$$\sum_{i\in In^k} m_{i,t}^{pipe} - \sum_{j\in Lv^k} m_{j,t}^{pipe} = m_{k,t}^{node} \tag{4}$$

where $m_{i,t}^{pipe}$ is the mass flow of pipe i at time t, and $m_{k,t}^{node}$ is the mass flow of node k at time t for $k \in H^{node}$. H^{node} is the set of nodes in DHS. In^k and Lv^k are the sets of the pipes injecting into the node k and the pipes leaving from the node k, respectively.

Secondly, the pressure drop equation illustrates the sum of head pressure losses in a closed loop in DHS equals to zero

$$\sum_{k\in L} h_{i,t} = 0 \tag{5}$$

where $h_{i,t}$ is the head loss of pipe i at time t for $i \in H^{pipe}$ and L is the set of loops. H^{pipe} is the set of pipes in DHS.

Thirdly, the head loss equation denotes the head loss of a pipe

$$h_{i,t} = K_{i,t} \left| m_{i,t}^{pipe} \right| m_{i,t}^{pipe} \tag{6}$$

where $K_{i,t}$ is pipe resistance coefficient of pipe i at time t, and the calculation of $K_{i,t}$ is detailed in [38].

Here we introduce the node-branch incidence matrix $\boldsymbol{A}$ and the loop-branch matrix $\boldsymbol{B}$ [27], which are determined by DHS topology. The hydraulic model can be expressed using matrix form

$$\boldsymbol{A}\, \boldsymbol{m}_t^{pipe} = \boldsymbol{m}_t^{node} \tag{7}$$

$$\boldsymbol{B}\, \boldsymbol{h}_t = \boldsymbol{0} \tag{8}$$

$$\boldsymbol{h}_t = \boldsymbol{K}_t \left| \boldsymbol{m}_t^{pipe} \right| \boldsymbol{m}_t^{pipe} \tag{9}$$

where $\boldsymbol{m}_t^{pipe}$ and $\boldsymbol{m}_t^{node}$ are vectors of the pipe and the node mass flow at time t respectively. $\boldsymbol{h}_t$ is the head loss vector, and $\boldsymbol{K}_t$ is the pipe resistance vector.

2.3.2 Dynamic Thermal Network Model

Since the time scale of the thermal process in DHS varies from several minutes to hours, the dynamic thermal model is formulated in this section to track heat dynamic process.

Fig. 3 presents the structure of the thermal model and the relationship between model equations, which indicates that the thermal model is based on the pipe heat conductive equation and node temperature mixing equations [27][39]. The former equation is a partial differential equation that describes temperature dynamics and time delay in heat dynamic process, and we transform it into solvable model by simplifying the differential term and applying the finite difference method. The latter equations, which link pipes (branches) and nodes together as a network, are a set of nonlinear equations which reflect the coupling of hydraulic variables and thermal variables in heat transmission process.

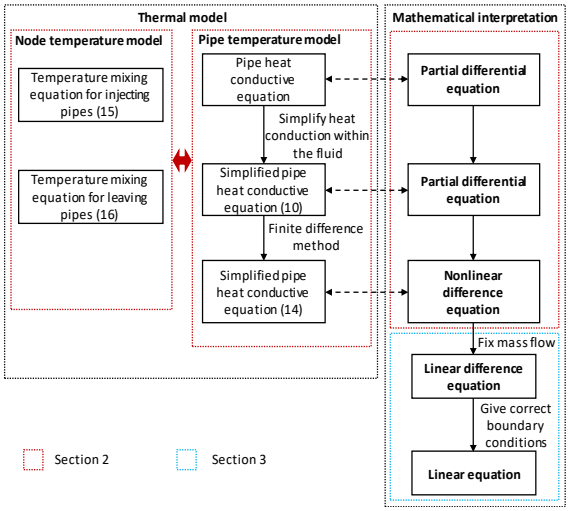

Fig. 3. The relationship of different equations in thermal model.

The first equation i.e. pipe heat conductive equation describes the temperature distribution in pipes [26][27]

$$\rho C_p A_i \frac{\partial T_i^{pipe}(x,t)}{\partial t} + m_i^{s,pipe}(x,t)\cdot C_p \frac{\partial T_i^{pipe}(x,t)}{\partial x} = kA_i \frac{\partial^2 T_i^{pipe}(x,t)}{\partial x^2} + \frac{T_i^a - T_i^{pipe}(x,t)}{R_i}$$

where $T_i^{pipe}(x,t)$ and $m_i^{pipe}(x,t)$ are the pipe temperature and the mass flow at time t and distance x from pipe initial point for $i \in H^{pipe}$. Since the hydraulic process is in the steady state, pipe mass flow is same everywhere i.e. $m_i^{pipe}(x,t) = m_{i,t}^{pipe}$. k, ρ and C_p are thermal conductivity, density and capacity of water. A_i and R_i are the cross-sectional area and the thermal conductive coefficient of pipe i, respectively.

Since the heat conduction within the fluid can be neglected, the partial differential term on the left side of the above heat conductive equation is omitted [26][27]

$$\rho C_p A_i \frac{\partial T_i^{pipe}(x,t)}{\partial t} + m_{i,t}^{pipe} C_p \frac{\partial T_i^{pipe}(x,t)}{\partial x} = \frac{T_i^a - T_i^{pipe}(x,t)}{R_i} \tag{10}$$

Using Taylor expansion and finite difference method [40], we get

$$\frac{\partial T_i^{pipe}(x,t)}{\partial t} = \frac{T_i^{pipe}(x,t) - T_i^{pipe}(x,t-\Delta t)}{\Delta t} \tag{11}$$

$$\frac{\partial T_i^{pipe}(x,t)}{\partial x} = \frac{T_i^{pipe}(x,t) - T_i^{pipe}(x-\Delta x,t)}{\Delta x} \tag{12}$$

where Δt and Δx are time and length segments for pipes, respectively. The choice of the segments should satisfy

$$\Delta x_{\min} \geq \frac{m_{i,t}^{pipe}\Delta t}{A_i \rho} \tag{13}$$

where (13) is for $\forall i \in H^{pipe}$.

Finally substitute (11) and (12) into (10). The partial differential equation (10) is transformed into the nonlinear algebraic equation in (14) [27].

$$T_i^{pipe}(x,t) = \frac{1}{\frac{1}{\Delta t} + \frac{m_{i,t}^{pipe}}{\Delta x \rho A_i} + \frac{1}{\rho C_p A_i R_i}} \left(\frac{T_i^a}{\rho C_p A_i R_i} + \right.$$
$$\left. + \frac{m_{i,t}^{s,pipe}}{\Delta x \rho A_i} T_i^{pipe}(x-\Delta x,t) + \frac{1}{\Delta t} T_i^{pipe}(x,t-\Delta t) \right) \tag{14}$$

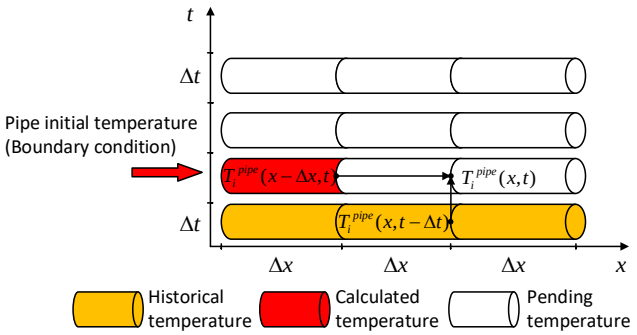

Fig. 4. The physical illustration of pipe temperature calculation in proposed quasi-dynamic model.

Fig. 4 presents the physical illustration of (14), which indicates that the current temperature is calculated by not only the current state but also former state. Hence, if the boundary condition (pipe initial temperature $T_{i,t}^{s,pipe}$) and pipe mass flow $m_{i,t}^{pipe}$ are given, we can calculate the pipe temperature distribution in a pipe according to (14).

Secondly, if more than two pipes inject into node *j*, temperature mixing equations are applied to calculate node temperature $T_{j,t}^{node}$

$$T_{j,t}^{node} = \frac{1}{\sum_{i \in In^j} m_{i,t}^{pipe}} \sum_{i \in In^j} T_{i,t}^{e,pipe} m_{i,t}^{pipe} \tag{15}$$

where the *j* is for $j \in H^{node}$, and $T_{i,t}^{e,pipe}$ is the terminal temperature of pipe *i* for $i \in In^j$ before mixing. Eq. (15) in the supply network of DHS indicates that the node temperature is the weighted mean of terminal temperature of injecting pipes. In return network, the injecting pipes include the node return pipelines.

The initial temperature of leaving pipe $T_{i,t}^{s,pipe}$ equals to the temperature of the node connected to the pipe initial point $T_{j,t}^{node}$

$$T_{i,t}^{s,pipe} = T_{j,t}^{node} \tag{16}$$

where $T_{i,t}^{s,pipe}$ is the initial temperature of pipe *i* for $j \in H^{pipe}$. Above equations can be applied in both supply and return network.

2.3.3 Node Model in DHS

The node in DHS is modeled as the heat exchanger [14][41][42], where the heat power of the heat source or load node in DHS is calculated by

$$\Phi_{i,t} = C_p m_{i,t}^{node} (T_{i,t}^{s,node} - T_{i,t}^{r,node}) \tag{17}$$

where $\Phi_{i,t}$ is the heat power of node *i* at time *t*. Eq. (17) indicates that the hydraulic variable $m_{i,t}^{node}$ and the thermal variables, including node supply temperature $T_{i,t}^{s,node}$ and return temperature $T_{i,t}^{r,node}$, are coupled by heat power at nodes. In the supply network, $T_{i,t}^{s,node} = T_{i,t}^{node}$, and in return network, $T_{i,t}^{node}$ is calculated from $T_{i,t}^{r,node}$ [20].

3. Calculation Method: HE-FBI Method

3.1 Basic Idea

The quasi-dynamic IES model is complicated because it couples nonlinear equations and difference equations which need accurate boundary conditions. Physically, in IES, the EPS and the DHS has diverse characteristics and only couples at sources, thus we can decompose EPS and DHS and calculate them iteratively. Furthermore, in DHS, the direction-variable hydraulic mass flow decides the boundary conditions of Eq. (14) and the formulation of Eq. (15). The coupling of mass flow and temperature in Eq. (15) and Eq. (17) causes nonlinearity.

To overcome these challenges, we use the fixed-point iteration to fix temperature in hydraulic calculation and fix mass flow in thermal calculation. Then the iteration of hydraulic and thermal calculation updates variables until convergence is achieved.

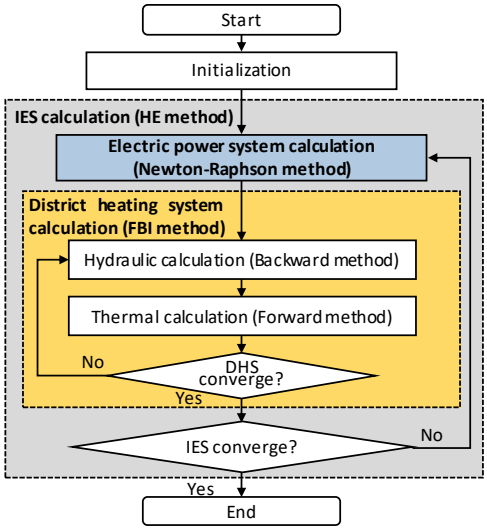

Fig. 5. Flow chart of HE-FBI method.

Based on above ideas and the framework in [20][38], in this section, a solving method called Heat-Electric Iteration with Forward-Backward Iteration (HE-FBI) method is proposed to solve the equations of the quasi-dynamic model and calculate the IES power flow, where the algorithms are

changed compared with [20] and [38]. As illustrated in the gray block of Fig. 5, the "HE" indicates Heat-Electric iteration which solves the electric-heat coupling for the whole IES. As presented in the yellow block in Fig.5, the "FBI" indicates the Forward-Backward Iteration in DHS which deals with hydraulic-thermal coupling.

Mathematically, the HE-FBI method decomposes complicated system equations into small parts according to the physical nature of different subsystems and solves them sequentially and iteratively. In terms of the challenges in IES, the HE-FBI method overcomes the complexity caused by the nonlinearity, the coupling of algebraic equations and difference equations and the changing forms of the temperature mixing equation in DHS.

3.2 Assumptions

To solve the IES equations and calculate power flow, several assumptions are clarified in HE-FBI method, which are illustrated in Table 4.

Table 4

Assumptions of Proposed Model

Type	Assumptions
Network topology	arbitrary
Mass flow in DHS	variable (including direction)
Media	water
Node type (Boundary condition)	3 types

Three types of node in EPS and DHS are presented in Table 5 according to the operating and control mechanism of different DERs [26,30,33-34].

Table 5

Node Types in EPS and DHS

EPS node (bus) type	DHS node type	Example
PV node	ΦT_s node	Generator (CHP unit)
PQ node	ΦT_r node	Load user
Slack node ($V\theta$ node)	Slack node (hT_s node)	Slack generator

where the *h* is node head pressure. The node types are named by the known variables at the nodes.

3.3 Heat-Electric Iteration in IES

As shown in the gray block at Fig. 5, the Heat-Electric (HE) iteration for the IES is applied to decompose the calculation of EPS and DHS by fixing and iterating the boundary conditions until converging [20].

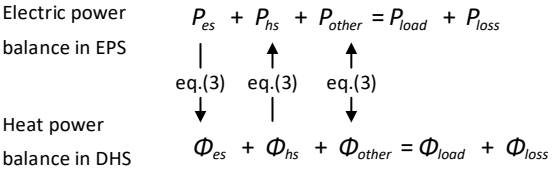

Fig. 6. Illustration of Heat-Electric iteration process.

Considering the EPS and the DHS each have one slack node respectively, in Fig. 6, the steps of the HE iteration are

1. Decide the electric power outputs P_{other} and the heat power outputs Φ_{other} of non-slack generator nodes using heat-electric coupling equation (3).
2. Calculate electric power flow in EPS and compute the heat power Φ_{es} of the electric slack node from the electric power P_{es} of the electric slack node by heat-electric coupling equation (3).
3. Calculate heat power flow in DHS and compute the electric power P_{hs} of the heat slack node from the heat power Φ_{hs} of the heat slack node by heat-electric coupling equation (3).

The electric and heat power outputs in step 1 are given conditions which can be provided by economic dispatch or other mechanisms. The iteration of step 2 and step 3 continues until heat and electric power outputs of two slack nodes converge. Thus, the IES power flow is obtained by solving model equations The concrete calculation methods for the EPS and the DHS are shown in the following text.

3.4 EPS Calculation: Newton-Raphson Method

To calculate the nonlinear electric power flow equations, the well-known Newton-Raphson method is applied in EPS with arbitrary topology. The iterative form of the Newton-Raphson method is

$$\begin{bmatrix} \boldsymbol{V} \\ \boldsymbol{\theta} \end{bmatrix}^{k+1} = \begin{bmatrix} \boldsymbol{V} \\ \boldsymbol{\theta} \end{bmatrix}^{k} + \left(\boldsymbol{J}_e^{-1} \begin{bmatrix} \boldsymbol{\Delta Q} \\ \boldsymbol{\Delta P} \end{bmatrix} \right)^{k} \tag{18}$$

where *k* indicates the iteration times. $\boldsymbol{V}$ and $\boldsymbol{\theta}$ are the vectors of node voltage and phase angle respectively, and the $\boldsymbol{J}_e^{-1}$ is the Jacobian matrix in EPS. $\boldsymbol{\Delta Q}$ and $\boldsymbol{\Delta P}$ are active and reactive power mismatch respectively [34][44].

3.5 DHS Calculation: Forward-Backward Iteration

The Forward-Backward Iteration (FBI) method is proposed to deal with the complexity in DHS, including nonlinearity, the coupling of algebraic equations and difference equations and changing forms of temperature mixing equation. The Fig. 7 is the flow chart of the FBI method.

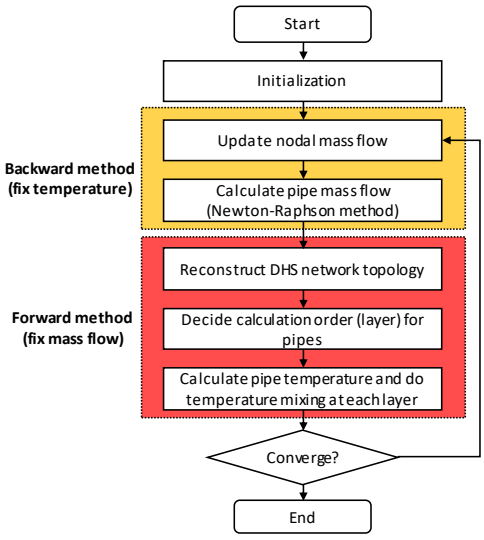

Fig. 7. Flow chart of Forward-Backward Iteration method.

The FBI method applies the fixed-point method to overcome the complexity in DHS and has the similar idea with the forward-backward sweep method in EPS. For better understanding, the comparison is presented in Table 6. The nonlinearity in the hydraulic model is solved by the Newton-Raphson method. Then the Forward method fixes mass flow to linearize difference equation (14), gives correct pipe boundary conditions and updates temperature mixing node dynamically according to the mass flow, which decides the form of temperature mixing equations .

3.5.1 Backward Method for Hydraulic Model

The Backward method is proposed to calculate the hydraulic model for arbitrary DHS network with multiple DERs, meshed network and variable mass flow. In the Backward method, variables of node supply and return temperature ($T_{i,t}^{s,node}$ and $T_{i,t}^{r,node}$) are fixed, thus, node mass flow m_t^{node} can be calculated from Eq. (17). Then the problem is transferred to calculate pipe mass flow vector $\boldsymbol{m}_t^{pipe}$ from node mass flow vector $\boldsymbol{m}_t^{node}$.

After that, the Newton-Raphson method is applied to solve pipe mass flow from the nonlinear equations (7)-(9) [27]

$$\left(\boldsymbol{m}_t^{pipe}\right)^{k+1}=\left(\boldsymbol{m}_t^{pipe}\right)^{k}-\left(\boldsymbol{F}_h\right)^{k}=\left(\boldsymbol{m}_t^{pipe}\right)^{k}-\left(\boldsymbol{J}_h^{-1}\Delta\boldsymbol{F}_h\right)^{k} \quad (19)$$

where k indicates the iteration times, $\boldsymbol{J}_h$ is the Jacobian matrix in the hydraulic calculation, and $\Delta\boldsymbol{F}_h$ is the hydraulic mismatch vector in which

$$\boldsymbol{J}_h=\begin{bmatrix}\boldsymbol{A}_r\\ 2\boldsymbol{B}\boldsymbol{K}\left|\boldsymbol{m}_t^{pipe}\right|\end{bmatrix} \quad (20)$$

$$\Delta\boldsymbol{F}_h=\begin{bmatrix}\boldsymbol{A}_r\boldsymbol{m}_t^{pipe}-\boldsymbol{m}_{r,t}^{node}\\ \boldsymbol{B}\boldsymbol{K}\boldsymbol{m}_t^{pipe}\left|\boldsymbol{m}_t^{pipe}\right|\end{bmatrix}$$

where $\boldsymbol{m}_{r,t}^{node}$ is the reduced node mass flow vector which eliminates the mass flow of heat slack node, and $\boldsymbol{A}_r$ is the reduced node-branch matrix with the dimension of $(n_{node}-1)\times n_{pipe}$ after eliminating the heat slack node in DHS. $\boldsymbol{A}_r$ in the supply and return network has opposite directions. The dimension of $2\boldsymbol{B}\boldsymbol{K}\left|\boldsymbol{m}_t^{pipe}\right|$ is $n_{loop}\times n_{pipe}$ [38]. And the n_{pipe} , n_{node} and n_{loop} are the number of the pipelines, nodes and loops in DHS respectively.

Additionally, if there is no loop in a DHS (the DHS network is radial), the hydraulic model only has Eq. (7), and this linear equation can be directly solved. The Backward method is same in the supply network and the return network of the DHS.

3.5.2 Forward Method for Thermal Model

The Forward method is developed to track the thermal dynamic process by solving difference equations sequentially based on the physical nature.

In Forward method, the mass flow is fixed. Thus Eq. (14) and (15) become linear difference equations. In the supply network of DHS, the node and pipe temperatures are calculated sequentially by

1. Reconstruct the DHS network at time t by adjusting the defined direction of pipes whose mass flow $m_{i,t}^{pipe}$ is less than zero.
2. Decide the calculation order (layer) of pipelines:

$$L_i=\begin{cases}1 & \text{if } n_i^s\in\varphi\\ k+1 & k=\max\{L_j\mid n_j^e=n_i^s\},n_i^s\notin\varphi\end{cases} \quad (21)$$

   where L_i is the layer number of pipe i, which indicates the calculation order. φ is the set of all heat source nodes (ΦT_s nodes and hT_s node), n_i^s is the starting node of pipe i, and n_j^e is the ending node of pipe j in the reconstructed network. The first row of (21) indicates that L_i=1 if the pipe i is connected to the heat source. The second row of (21) means that the layer number of pipe i is decided by the maximum layer number of its injecting pipe j, i.e. L_j, where $n_j^e=n_i^s$ indicates the relationship between pipe i and j.
3. In each layer, calculate the terminal temperature of pipes using (14) and then calculate the temperature of mixing nodes based on (15) and (16). This step is implemented layer by layer.

For the return network in DHS, the step 1 and the step 3 are same, and the difference is to change φ to ψ which implies the set of all heat load nodes (ΦT_r nodes) in step 2.

Remark 1: The step 1 enables pipes with the negative mass flow to have correct boundary conditions while calculating (14). If no adjustment is made, when mass flow $m_{i,t}^{pipe}$ of pipe i is less than zero at time t, the pipe initial temperature is not the given boundary condition. As a result, the calculation of pipe i will not have correct results.

Remark 2: The step 2 ensures that the boundary condition of (14) is satisfied for each pipe when calculating pipes sequentially according to the layer L_i in DHS with multiple DERs and the meshed network topology.

Table 6

Comparison of the proposed FBI method and forward-backward sweep method in EPS

	Similarities		**Differences**	
	Forward Process	Backward Process	Direction	Topology
Proposed FBI method	calculate temperature with fixed mass flow	calculate mass flow with fixed temperature	mass flow cannot be negative	Topology reconstructing
Forward-backward sweep method in EPS	calculate voltage drop with fixed current	calculate current with fixed voltage	current can be negative	Fixed

After finishing Forward method, node supply and return temperature ($T_{i,t}^{s,node}$ and $T_{i,t}^{r,node}$) and the pipe temperature distribution $T_i^{pipe}(x,t)$ are calculated. Then the results are sent to the backward method to update new node mass flow using Eq. (17). If the maximum node mass flow difference of k and k+1 time iteration converges to a given positive value ε_h ,

$$\max\left|\frac{\left(m_{i,t}^{node}\right)^{(k+1)}-\left(m_{i,t}^{node}\right)^{(k)}}{\left(m_{i,t}^{node}\right)^{(k)}}\right|\le\varepsilon_h \tag{22}$$

the FBI method obtains the DHS power flow, including node supply and return temperature, pipe mass flow, the power output at heat slack node and the pipe temperature distribution $T_i^{pipe}(x,t)$ which can be used to quantify the storage capacity of DHS pipelines for accepting more renewables.

Additionally, the proposed FBI method can be applied in the DHS with different node types (see Section 3.2 assumptions). For example, if the second node type in DHS (i.e. the ΦT_r node for load users) is changed to $\Phi\,\Delta T$ node at which the given condition is the heat power Φ and the difference of node supply and return temperature ΔT , the node mass flow $\boldsymbol{m}_t^{node}$ can be directly calculated from (17) by the Backward method. Thus, the DHS calculation can be finished by one step of the FBI method.

Remark 3: The judgment (22) is the per-unit difference which can avoid the inaccuracy and inefficiency caused by directly using the original value of mismatch [14][20], especially when the mass flow of heat source nodes is much larger than the mass flow of heat load nodes.

4. Convergence Analysis of DHS Calculation

To illustrate the computational stability of the proposed DHS model, the calculation convergence is analyzed in this section compared with existing steady-state model [20] [38], where both methods in DHS calculation are based on the fixed-point method.

4.1. Convergence Theorem

In the hydraulic calculation i.e. Backward method, the node supply and return temperature ($T_{i,t}^{s,node}$ and $T_{i,t}^{r,node}$) are fixed to calculate the pipe mass flow $m_{i,t}^{pipe}$; in thermal calculation i.e. Forward method, the pipe mass flow $m_{i,t}^{pipe}$ is fixed to calculate node supply and return temperature ($T_{i,t}^{s,node}$ and $T_{i,t}^{r,node}$). The two calculation processes are iterated by (17) until converge. Thus, the convergence condition for the above fixed-point iteration is [45]

$$|\nabla f|\cdot|J_h|\le 1 \tag{23}$$

where $|J_h|$ is the 1 norm of the Jacobian matrix of hydraulic calculation in (20), and $|\nabla f|$ is the 1 norm of the partial derivative of the pipe temperature with respect to mass flow, in which

$$\nabla f=\frac{\partial \boldsymbol{T}^{pipe}(x,t)}{\partial \boldsymbol{m}_t^{pipe}} \tag{24}$$

where $\boldsymbol{T}^{pipe}(x,t)$ is the vector of pipe temperature distribution function $T_i^{pipe}(x,t)$.

4.2. Mathematical Analysis Based on Simple DHS

This section is designed to analyze the convergence characteristics of the proposed quasi-dynamic model mathematically compared with the existing steady-state model [20] [38]. The analysis bases on the DHS in Fig. 8 where node 1 is a heat slack node, and node 2 is a ΦT_r node.

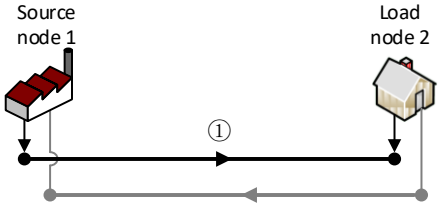

Fig. 8. Test DHS for convergence analysis.

Assuming that the length of pipe 1 is short enough:

$$0<L_1=\Delta x \tag{25}$$

then the pipe terminal temperature of pipe 1 is the nodal supply temperature of node 2, which indicates

$$T_1^{pipe}(L_1,t)=T_{2,t}^{node} \tag{26}$$

Thus, the temperatures of node 1 at time t and node 2 at time $t-\Delta t$ have little difference, which implies

$$\left|T_{1,t}^{node}-T_{2,t\text{-}\Delta t}^{node}\right|<\delta \tag{27}$$

where the δ is a small temperature difference and generally is less than 5°C if the Δt is not too large, because the sharp change of temperature seldom happens in DHS [26]. The reduced node-branch matrix $\boldsymbol{A}_r$ of the Fig. 8 is

$$\boldsymbol{A}_r=[1]_{1\times 1} \tag{28}$$

And the loop-branch matrix $\boldsymbol{B}$ does not exist because of the absence of loops.

For the proposed quasi-dynamic model, substitute (14) and (26) to (24)

$$\nabla f_d=\frac{\dfrac{T_{1,t}^{node}-T_{2,t\text{-}\Delta t}^{node}}{\Delta t\Delta x\rho A_p}+\dfrac{T_{1,t}^{node}-T_a}{\Delta x\rho^2 A_p^2 C_p R}}{\left(\dfrac{1}{\Delta t}+\dfrac{m_{1,t}^{pipe}}{\Delta x\rho A_p}+\dfrac{1}{\rho C_p A_p R}\right)^2} \tag{29}$$

where ∇f_d is the 1 norm of the partial derivative of temperature with respect to mass flow in the proposed quasi-dynamic model.

The steady-state model applies the simplified pipe conductive equation without heat dynamic process

$$T_1^{pipe}(x,t)=(T_{1,t}^{node}-T_a)e^{-\frac{Rx}{C_p m_{1,t}^{pipe}}}+T_a \tag{30}$$

Substitute (14) and (30) into (24)

$$\nabla f_s=(T_{1,t}^{node}-T_a)e^{-\frac{RL}{C_p m_{1,t}^{pipe}}}\left(\frac{RL}{C_p}\right)\frac{1}{\left(m_{1,t}^{pipe}\right)^2} \tag{31}$$

where ∇f_s is the 1 norm of the partial derivative of temperature with respect to mass flow in steady-state model.

In the proposed quasi-dynamic model and the steady-state model, the hydraulic models are the same, and the Jacobian matrix is

$$J_{h,d}=J_{h,s}=1 \tag{32}$$

where "1" in the right hand is a scalar, and the $J_{h,d}$ and $J_{h,s}$ are Jacobian matrices of the proposed quasi-dynamic and the steady-state model, respectively.

Choosing $\Delta t = 15$, $\Delta x = 5$ and $A_1 = 1$ which satisfy the constraint (13) from experience [26], we have

$$\nabla f_d = \frac{\frac{T_{1,t}^{node} - T_{2,t-\Delta t}^{node}}{2335} + \frac{T_{1,t}^{node} - T_a}{2070516}}{\left(\frac{1}{15} + \frac{m_{1,t}^{pipe}}{157} + \frac{1}{13188}\right)^2} < \frac{\frac{\delta}{2335}}{\left(\frac{1}{15}\right)^2} << 1$$

$$\nabla f_s = \frac{1}{46.67\left(m_{1,t}^{pipe}\right)^2}$$

For the proposed quasi-dynamic model, even when the pipe mass flow is zero, $|\nabla f_d||J_{h,d}|$ is much less than 1, which means that the proposed quasi-dynamic model is robust. But for the steady-state model, while the pipe mass flow $m_{1,t}^{pipe}$ is less than 0.416 kg/s, the $|\nabla f_d||J_{h,d}|$ will be larger than 1, which cannot ensure the convergence. So we can conclude that under the given conditions, the steady-state model has convergence problems with slow mass flow, while the proposed quasi-dynamic model is robust even when the mass flow is zero.

4.3. Tests on Convergence Performance in Complex DHS

This section aims to extend the convergence analysis from the simple DHS to the complex DHS by applying numerical tests to reveal the physical causation. The analysis is based on the DHS in a real IES situated in Barry Island, South Wales [38][46], which is shown in Fig. 9.

The Fig. 10 and the Fig. 11 present the results of the proposed quasi-dynamic model and the steady-state model, including the mass flow at one node and the per-unit difference between two hydraulic-thermal iterations. The stopping criteria for convergence are that the maximum node mass flow difference between two iterations is less than 10^{-3} p.u. i.e. $\varepsilon_h = 10^{-3}$ p.u. in Eq. (22)

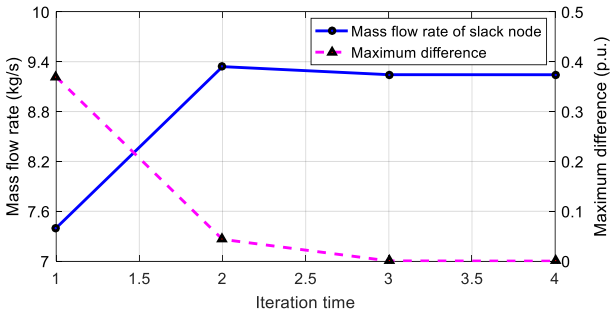

Fig. 10. Mass flow of heat slack node and maximum difference between two iterations of the proposed quasi-dynamic model.

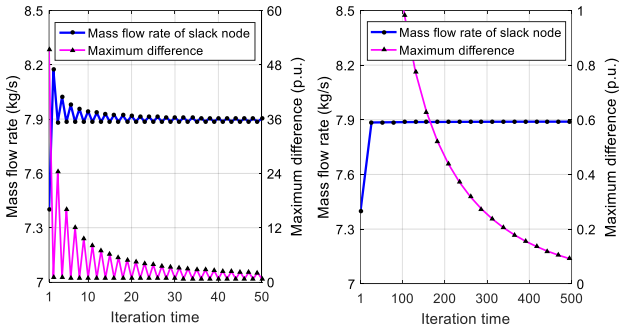

Fig. 11. Mass flow of heat slack node and maximum difference between 2 iterations of steady-state model for (a) 20 iterations and (b) 500 iterations.

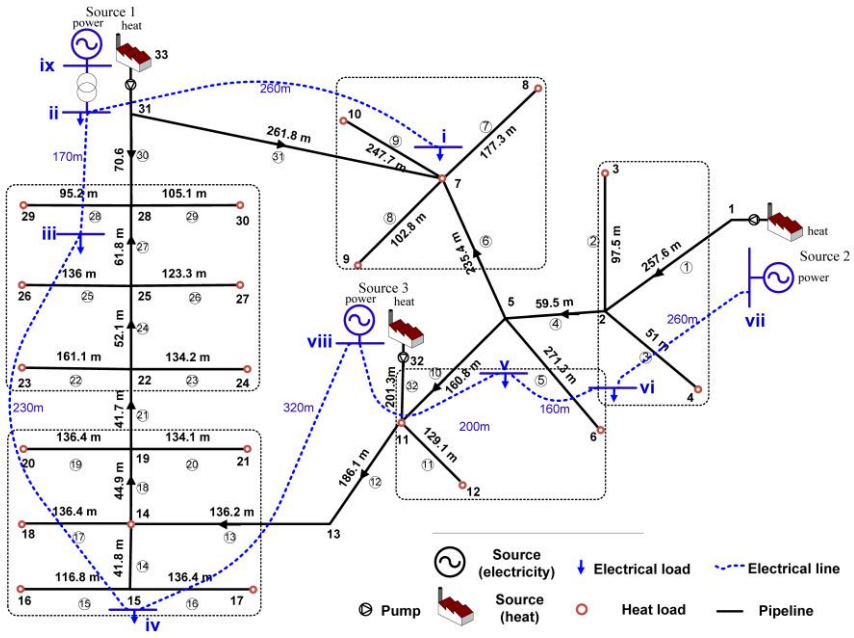

Fig. 9. The IES with EPS and DHS in Barry Island.

It can be observed from Fig. 10 that the proposed quasi-dynamic model converges after 4 iterations, but in Fig. 11 the steady-state model does not converge after 20 iterations and has the large difference. Even after 500 times, the steady-state model does not converge. To explain the reason of the above phenomenon, the physical explanations of the two models are presented in Fig. 12, where n and n_{max} are iteration time and maximum iteration time respectively. For better understanding, the physical illustrations of the pipe temperature calculation of the proposed model and steady-state model are compared in Fig. 13.

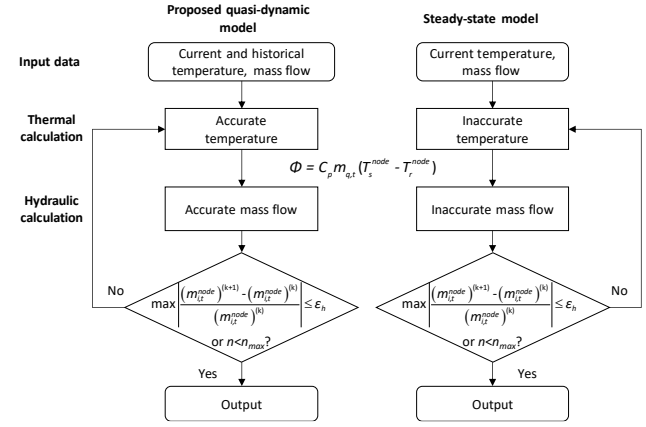

Fig. 12. The physical illustration of the calculation process in proposed quasi-dynamic model and steady-state model

In Fig. 13 (a), the proposed quasi-dynamic model uses both current state and historical state of pipes i.e. pipe historical temperature distribution to calculate current temperature results because the thermal process is still in dynamics. Thus, the temperature results are accurate in the thermal calculation (Forward method), and then in the iteration process, it provides the hydraulic calculation (Backward method) with an accurate iteration point. As a result, the DHS calculation can converge to the solutions quickly and accurately in the proposed model.

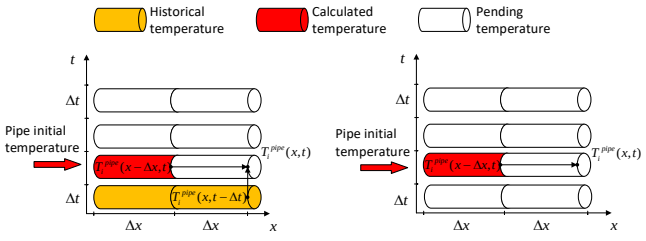

Fig. 13. The comparison of pipe temperature calculation in (a) proposed quasi-dynamic model and (b) steady-state model.

However, the steady-state model in Eq. (30) and Fig. 13 (b) simplifies the pipe thermal model by neglecting the influence from historical temperature and only uses the current state to calculate current temperature results, thus ignoring the heat dynamic process. Therefore, the temperature results of the steady-state model are not accurate, and then the inaccuracy is transmitted to the hydraulic calculation of mass flow by the fixed-point method (17). As a result, in the steady-state model, the "chain of inaccuracy" may lead to the non-convergence of IES power flow calculation.

To validate the computational stability of the proposed quasi-dynamic model from another angle, we design different scales of DHS from 5-node system to 119-node system. As shown in Fig. 14, the maximum node mass flow differences between two iterations are less than the given convergence difference ε_h =10^{-3}, which indicates the proposed model can converge in the calculation of different scales of DHS. Furthermore, the average difference of 50 calculation points from 0:00 to 02:30 is below 2.2×10^{-4} p.u., demonstrating the good convergence characteristics and the accuracy of the proposed model.

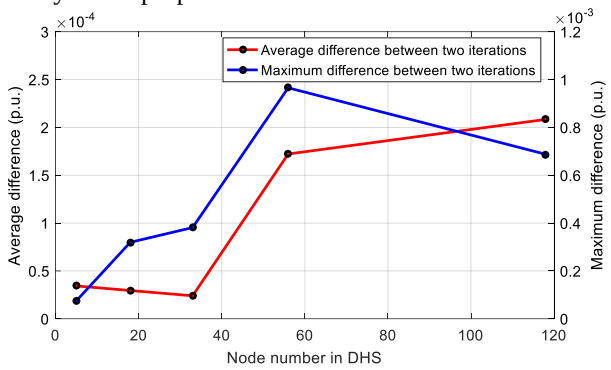

Fig. 14. The maximum difference and average difference between two iterations in different DHS

In brief, the proposed quasi-dynamic model improves the convergence and accuracy by using the dynamic heat conductive equation which bases on the physical nature of DHS.

Remark 4: Limited to direction-variable mass flow, the strict boundary condition of pipe temperature calculation in (14) and the coupling of algebraic equations and difference equations, the function of the DHS cannot be expressed analytically and use (23) or other methods such as Laplace transformation to analyze.

5. Case Study

Based on the data from the real world, literature and commercial software, the case studies are carried out to validate the proposed quasi-dynamic model and demonstrate the innovation of this research compared with existing research.

5.1. Case 1: Validation Using Real-World DHS Data

To verify the proposed model in DHS dynamic process, in which the DHS variables are time-varying, and the system does not reach steady-state, this case compares the calculated data of the proposed model and the measured data of a real DHS in Fig. 15 located in the suburb of Shijiazhuang, China [25]. The hot water is transported from the Luhua CHP unit to the heat exchanger station through the 9.25 km pipeline, where the supply temperature of the Luhua CHP unit and mass flow are variable.

The validation applies the measured supply temperature at Luhua CHP unit and the mass flow to calculate the temperature at heat exchanger station using the proposed model, which is compared with the measured temperature at

heat exchanger station from 0:00 to 24:00 on Dec 15th, 2015 [25].

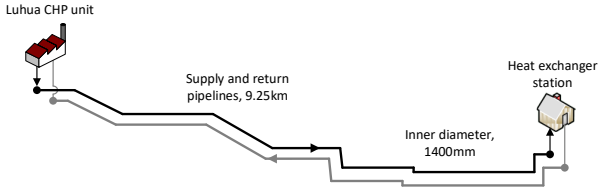

Fig. 15. Topology of the DHS in Shijiazhuang, China.

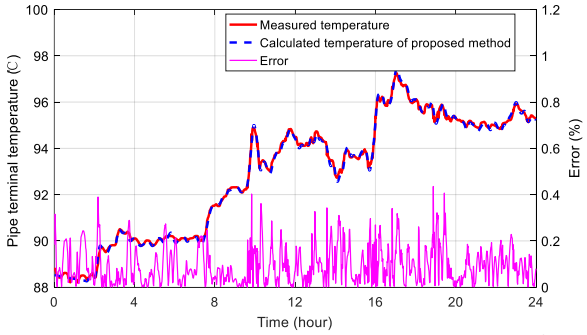

Fig. 16. The calculated pipe terminal temperature and the error of the proposed model and measured data.

Fig. 16 presents the results of the calculated pipe terminal temperature and the error of the proposed model and the measured data, which indicates that the proposed method has the average error of 0.09% (0.0864℃) and the maximum error of 0.44% (0.4148℃) compared with the measured data. Considering the structure of the real DHS, the error may come from the temperature sensor at heat exchanger station and the inaccurate estimation of the pipe parameter R and the environmental temperature T_a . Thus, the temperature calculated by the proposed method has tiny error compared with the measured data, demonstrating the effectiveness of the proposed DHS model.

5.2. Case 2: Dynamic Process in Test DHS

The Case 2 is designed to validate the proposed model in the dynamic process using the data from the commercial software *Bentley sisHYD*. The case is based on the meshed DHS network in Fig. 17 with two DERs and variable mass flow, and the detailed data of this case are uploaded in [47].

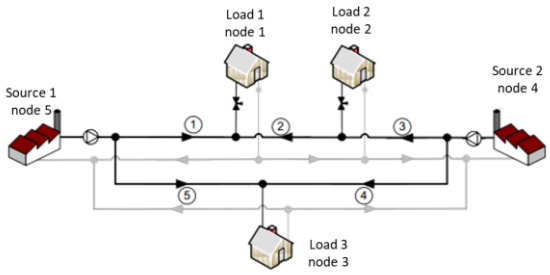

Fig. 17. DHS network topology of case 2.

In Fig. 17, the circled numbers are numbers of pipes, and the node numbers are below the names of sources or loads. The node 5 is a heat slack node while the node 4 is a ΦT_s node. Under the same conditions of the proposed quasi-dynamic model and the *Bentley sisHYD*, the pipe temperature results are shown from Fig.18a to Fig.18e.

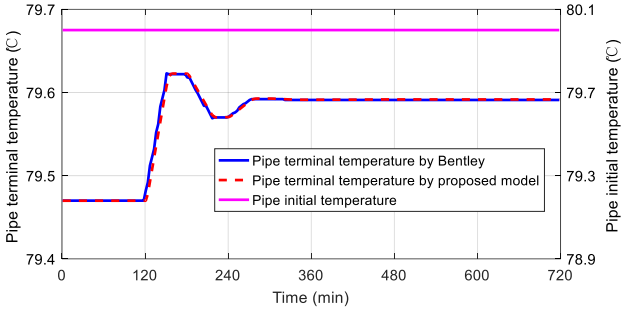

Fig. 18a. Pipe initial temperature and terminal temperature of pipe 1.

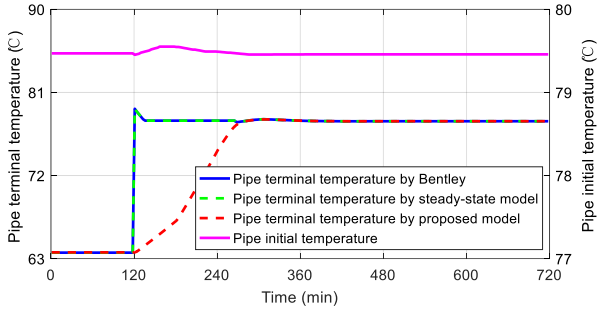

Fig. 18b. Pipe initial temperature and terminal temperature of pipe 2.

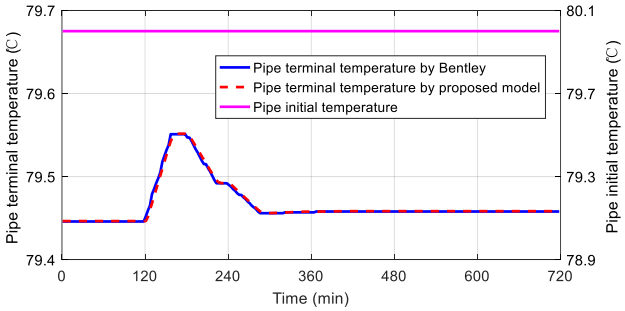

Fig. 18c. Pipe initial temperature and terminal temperature of pipe 3.

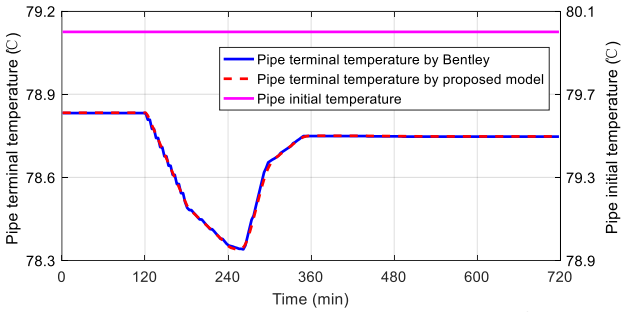

Fig. 18d. Pipe initial temperature and terminal temperature of pipe 4.

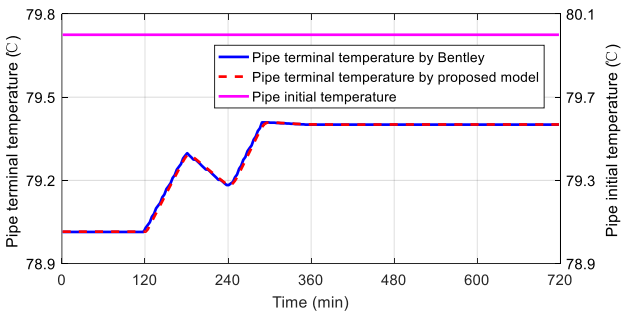

Fig. 18e. Pipe initial temperature and terminal temperature of pipe 5.

From the temperature results in Fig. 18, except for the pipe 2, the proposed quasi-dynamic model and the *Bentley sisHYD* have same pipe temperature results because these pipes are connected to heat sources, where the boundary conditions (pipe initial temperature) are the supply temperature of heat sources and are easy to obtain. However, if we observe pipe 2 from 120 minutes to 250 minutes, the result of *Bentley sisHYD* has a sharp increase of temperature with no time delays and temperature dynamics, failing to reflect the heat dynamic process. To explore the reason for this failure, the pipe terminal temperature calculated by the steady-state model [38] is presented using a green dotted line in Fig. 18b. Obviously the commercial heat dynamic calculation software *Bentley sisHYD* has the same results as the steady-state model which ignores heat dynamic process. One possible explanation is that the *Bentley sisHYD* cannot decide the accurate boundary condition of the pipe 2 while the mass flow is variable in the DHS with meshed network. Thus, the *Bentley sisHYD* compromises to apply steady-state results for pipe 2. Yet the proposed quasi-dynamic model applied HE-FBI method can attain correct boundary conditions and reflect temperature change accurately for pipe 2 in the dynamic process. In brief, under given conditions, the proposed quasi-dynamic model is valid and has better dynamic performance compared with the commercial software *Bentley sisHYD.*

5.3. Case 3: Steady-state Process in Barry Island

The aim of Case 3 is to validate the proposed electric-heat coupling IES model in the steady-state process, which indicates the loads and sources have no adjustment and dynamics. This case is based on the topology of Barry Island in Fig. 9 which has a 9-node EPS and a 33-node DHS with the meshed network and 3 DERs.

To verify the accuracy, the proposed quasi-dynamic IES model is compared with the steady-state IES model [20] using the same topology and data in [38]. The detailed data are uploaded in [47]. The power flows of EPS and DHS are analyzed simultaneously, and the bus voltage in EPS and node supply temperature in DHS are drawn in Fig. 19 and Fig. 20 respectively.

Fig. 19 shows that the bus voltages of the proposed quasi-dynamic model and the steady-state model are same with no error because of applying the same EPS model under the same conditions. Moreover, in Fig. 20 for the DHS, the comparison of two models and another commercial software SINCAL holds same results even though the DHS models are different, where the average errors of the proposed quasi-dynamic model are 0.0998% and 0.0997% compared with the steady-state model and SINCAL respectively [47]. The reason is that the steady-state model (30) simplifies the dynamic thermal model (10) by neglecting the partial derivative of time t i.e. ignoring the heat dynamic process. But in the steady-state process, the pipe temperature $T_i^{pipe}(x,t)$ has already reached steady state, indicating that the $T_i^{pipe}(x,t)$ has no relation with time t and is only a function of distance x

$$T_i^{pipe}(x,t) = T_i^{pipe}(x)$$

and the partial derivative of time t at (10) equals to zero exactly.

$$\frac{\partial T_i^{pipe}(x,t)}{\partial t} = 0 \tag{33}$$

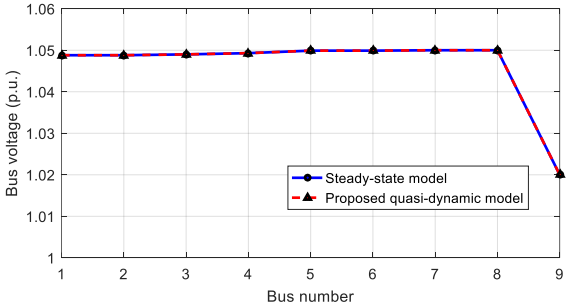

Fig. 19. Bus voltage of proposed quasi-dynamic model and steady-state model.

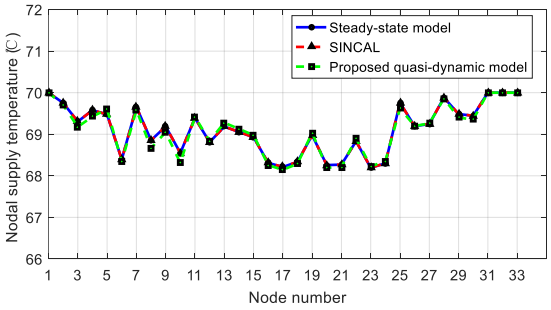

Fig. 20. Node supply temperature of proposed quasi-dynamic model, steady-state model and SINCAL in steady-state process.

Thus, Eq. (10), which reflect heat dynamic process, has changed to the form of (34), from which we can derive the steady-state model equation (30).

$$m_{i,t}^{pipe} \cdot C_p \frac{dT_i^{pipe}(x)}{dx} = \frac{T_i^a - T_i^{pipe}(x)}{R_i} \tag{34}$$

Therefore, although we simulate two disparate models in the steady-state process, the principles of the two models are same because of (33), demonstrating the effectiveness of the proposed quasi-dynamic model.

5.4. Case 4: Dynamic Process in Barry Island

Based on the IES topology in Fig. 9, Case 3 simulates the electric-heat coupling IES under the dynamic process. Because the EPS models in the existing steady-state IES model and the proposed quasi-dynamic IES model are same, and the difference of two models origins from the DHS model, the bus voltage is omitted and the node supply temperature is shown in Fig. 21.

It can be observed that in the dynamic process, as shown in Fig. 21, the two models have three main differences: time delay, temperature dynamics and convergence. Firstly, the light blue circle indicates the steady-state model fails to track time delays because of ignoring the dynamic heat transmission process. Secondly, circled by the red circle, the steady-state model does not converge at 4:45, 5:00, 20:30, and 21:00 because the steady-state thermal model transmits the inaccurate iteration point to hydraulic calculation, which

leads to the non-converge of the fixed-point iteration. Finally, as circled in the deep blue color, the steady-state model has unreasonable sharp temperature fluctuations as a result of ignoring heat dynamic process, failing to illustrate real temperature dynamics.

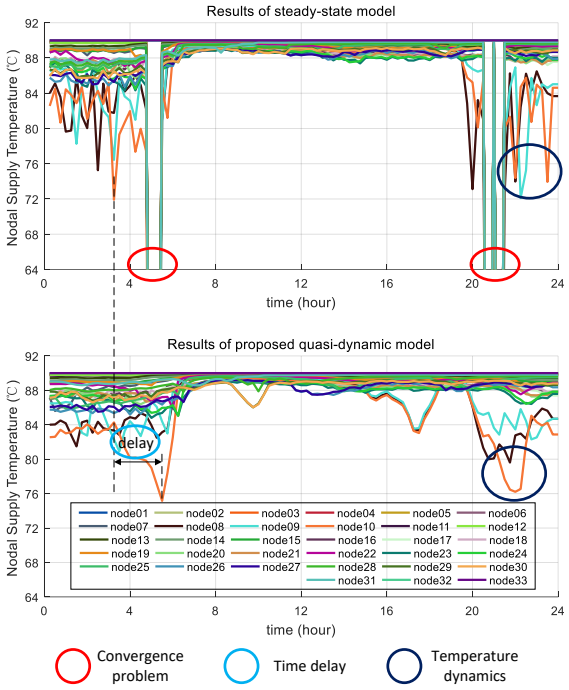

Fig. 21. Node supply temperature of proposed quasi-dynamic model and steady-state model in dynamic process.

In brief, it is essential to utilize the quasi-dynamic IES model in the dynamic process. Based on the energy system of Barry Island, the proposed quasi-dynamic model has better characteristics of convergence and reflecting heat dynamic process which is ignored by the steady-state model. Besides, the proposed quasi-dynamic model has high efficiency with the average calculation time of 1.40 seconds.

6. Conclusion

A quasi-dynamic model is proposed in electric-heat coupling IES considering heat dynamic process, meshed network, multiple DERs and variable mass flow simultaneously, which makes it widely applicable in solving real-world IES power flow problem. To overcome the difficulty of calculating complexity, the HE-FBI method is developed to decompose the model equations into small parts and solve them sequentially and iteratively based on the physical nature of IES. Mathematical and numerical convergence studies demonstrate that the proposed quasi-dynamic model improves convergence characteristics by providing the fixed-point method with reasonable iteration points compared with the steady-state model. In case studies, the average error of the proposed model and method is only 0.09% compared with the measured real data, which outperforms both the commercial software and the steady-state model. Moreover, it has also been proved by case studies that the heat dynamic process can be reflected, and better convergence can be guaranteed by the proposed quasi-dynamic model and HE-FBI method, which indicates the effectiveness and necessity of the research. Our future research topic will include the optimal power flow problem of IES considering the dynamic process in heating system.

Acknowledgements

This work is supported by the National Key R&D Program of China (2018YFB0905000), the National Natural Science Foundation of China (NSFC) (51537006), and the Science, Technology and Innovation Commission of Shenzhen Municipality (No. JCYJ20170411152331932).

References

[1] Wu J, Yan J, Jia H, Hatziargyriou N, Djilali, N, Sun, H. Integrated Energy Systems. Applied Energy 2016;167:155-157.

[2] Mancarella P. MES (multi-energy systems): An overview of concepts and evaluation models. Energy 2014;65:1-17.

[3] Sun H, Guo Q, Zhang B, Wu W, Wang B, Shen X. Integrated Energy Management System: Concept, Design, and Demonstration in China. IEEE Electrification Magazine 2018;6:42-50.

[4] Beigvand S D, Abdi H, La Scala M. Combined heat and power economic dispatch problem using gravitational search algorithm. Electric Power Systems Research 2016;133:160-172.

[5] Sepehri A, Sarrafzadeh M H. Effect of nitrifiers community on fouling mitigation and nitrification efficiency in a membrane bioreactor. Chemical Engineering and Processing-Process Intensification 2018;128:10-18.

[6] Riipinen M. District heating and cooling in Helsinki. In: Proceedings of the international CHP/DHC workshop. Paris. 2013. p. 12-13.

[7] Kang C, Chen X, Xu Q, Ren, D. Balance of power: toward a more environmentally friendly, efficient, and effective integration of energy systems in China. IEEE Power and Energy Magazine 2013;11:56-64.

[8] Rong A, Lahdelma R. An efficient model and algorithm for the transmission-constrained multi-site combined heat and power system. European Journal of Operational Research 2017;258:1106-1117.

[9] Foxon T J. Transition pathways for a UK low carbon electricity future. Energy Policy 2013,52:10-24.

[10] Pan Z, Guo Q, Sun H. Interactions of district electricity and heating systems considering time-scale characteristics based on quasi-steady multi-energy flow. Applied energy 2016;167:230-43.

[11] Sun H, Guo Q, Pan Z. Energy internet: concept, architecture and frontier outlook. Automation of Electric Power Systems 2015;39:1-8.

[12] Vesterlund M, Dahl J. A method for the simulation and optimization of district heating systems with meshed networks. Energy Conversion and Management 2015;89:555-567.

[13] Laajalehto T, Kuosa M, Mäkilä T, Lampinen M, Lahdelma R. Energy efficiency improvements utilising mass flow control and a ring topology in a district heating network. Applied thermal engineering 2014;69:86-95.

[14] Li Z, Wu W, Shahidehpour M, Wang J, Zhang B. Combined heat and power dispatch considering pipeline energy storage of district heating network. IEEE Transactions on Sustainable Energy 2016;7:12-22.

[15] Eladl A A, ElDesouky A A. Optimal economic dispatch for multi heat-electric energy source power system. International Journal of Electrical Power & Energy Systems 2019;110:21-35.

[16] Wang J, You S, Zong Y, Cai H. Investigation of real-time flexibility of combined heat and power plants in district heating applications. Applied Energy 2019;237:196-209.

[17] Geidl M. Integrated modeling and optimization of multi-carrier energy systems. ETH Zurich; 2007.

[18] Morvaj B, Evins R, Carmeliet J. Optimization framework for distributed energy systems with integrated electrical grid constraints. Applied energy 2016;171:296-313.

[19] Morvaj B, Evins R, Carmeliet J. Optimising urban energy systems: Simultaneous system sizing, operation and district heating network layout. Energy 2016;116:619-636.

[20] Liu X, Wu J, Jenkins N, Bagdanavicius A. Combined analysis of electricity and heat networks. Applied Energy 2016;162:1238-1250.

[21] Muditha A. Combined analysis of coupled energy networks. Phd thesis. Cardiff University; 2016.

[22] Pan G, Gu W, Wu Z, Lu Y, Lu S. Optimal design and operation of multi-energy system with load aggregator considering nodal energy prices. Applied Energy 2019;239:280-295.

[23] Sartor K, Dewalef P. Experimental validation of heat transport modelling in district heating networks. Energy 2017;137:961-8.

[24] Dahm J. District heating pipelines in the ground-simulation model; 1999.

[25] Wang Y, You S, Zhang H, Zheng, X , Zheng, W, Miao, Q. Thermal transient prediction of district heating pipeline: Optimal selection of the time and spatial steps for fast and accurate calculation. Applied Energy 2017;206:900-910.

[26] Duquette J, Rowe A, Wild P. Thermal performance of a steady state physical pipe model for simulating district heating grids with variable flow. Applied Energy 2016;178:383-93.

[27] Hassine IB, Eicker U. Impact of load structure variation and solar thermal energy integration on an existing district heating network. Applied Thermal Engineering 2013;50:1437-46.

[28] Pan Z, Wu J, Sun H, Guo Q, Abeysekera M. Quasi-dynamic interactions and security control of integrated electricity and heating systems in normal operations. CSEE Journal of Power and Energy Systems 2019;99:1-10.

[29] Lin C, Wu W, Zhang B, Sun Y. Decentralized Solution for Combined Heat and Power Dispatch Through Benders Decomposition. IEEE Transactions on Sustainable Energy 2017;8:1361-72.

[30] Gu W, Wang J, Lu S, Luo Z, Wu C. Optimal operation for integrated energy system considering thermal inertia of district heating network and buildings. Applied Energy 2017;199:234-246.

[31] Wang D, Zhi Y, Jia H, Hou K, Zhang S X, Du W, Fan M H. Optimal scheduling strategy of district integrated heat and power system with wind power and multiple energy stations considering thermal inertia of buildings under different heating regulation modes. Applied Energy 2019;240:341-358.

[32] Guelpa E, Verda V. Compact physical model for simulation of thermal networks. Energy 2019.

[33] Wang L X, Zheng J H, Li M S, Lin X, Jing Z X, Wu P Z, Zhou X X. Multi-time scale dynamic analysis of integrated energy systems: An individual-based model. Applied Energy 2019;237:848-861.

[34] Glover JD, Sarma MS, Overbye T. Power System Analysis & Design, SI Version: Cengage Learning; 2012.

[35] Bailey O, Creighton C, Firestone R, Marnay C, Stadler M. Distributed energy resources in practice: A case study analysis and validation of LBNL's customer adoption model. Office of Scientific & Technical Information Technical Reports; 2003.

[36] Zhao H. Analysis, modelling and operational optimization of district heating systems. PhD Thesis. Technical University of Denmark; 1995.

[37] Larock B E, Jeppson R W, Watters G Z. Hydraulics of pipeline systems. CRC press; 1999.

[38] Liu X. Combined analysis of electricity and heat networks. PhD Thesis. Cardiff University; 2013.

[39] Bergman T L, Incropera F P, DeWitt D P, Lavine A S. Fundamentals of heat and mass transfer. John Wiley & Sons; 2011.

[40] Vivian J, de Uribarri P M Á, Eicker U, Zarrella A. The effect of discretization on the accuracy of two district heating network models based on finite-difference methods. Energy Procedia 2018;149:625-634.

[41] Bøhm B, Kim W, Ha S, Kim B, Koljonen T, Larsen H, Wistbacka M. Simple models for operational optimisation. Contract; 2002.

[42] Zhao H. Analysis, Modelling and operational optimazation of district heating systems. Centre for District Heating Technology; 1995.

[43] Steer K C B, Wirth A, Halgamuge S K. Control period selection for improved operating performance in district heating networks. Energy and Buildings 2011;43:605-613.

[44] Seugwon A. Natural gas and electricity optimal power flow. PhD thesis. Oklahoma State University; 2004.

[45] Tan K K, Xu H K. Approximating fixed points of non-expansive mappings by the Ishikawa iteration process. Journal of Mathematical Analysis and Applications 1993;178:301-301.

[46] Y. Xing, A. Bagdanavicius, S. C. Lannon, M. Pirouti, and T. Bassett. Low temperature district heating network planning with the focus on distribution energy losses. In: The Fourth International Conference on Applied Energy (ICAE2012). Suzhou China; 2012.

[47] Data of case studies: https://cloud.tsinghua.edu.cn/d/aa00c8fb0f4e48799bd1/